SUPPLEMENTAL MATERIAL

Supplemental Table 1: GRK phosphorylation-deficient V1AR primers

Phospho-site	**Nucleotide mutations**	**Sequence** (sense top/antisense bottom)
S352	a1054g, g1055c	5'-gctgtaatccctggatatacatgttttttgctggccatctccttca-3' 5'-tgaaggagatggccagcaaaaaacatgtatatccagggattacagc-3'
S362	a1084g, g1085c	5'-ccttcaagactgtgttcaagccttcccatgctgccaaaac-3' 5'-gttttggcagcatgggaaggcttgaacacagtcttgaagg-3'
T378, S380	a1132g, a1138g, g1139c	5'-acatgaaggaaaaattcaacaaagaagatgctgacgctatgagcagaagacagacttttttattc-3' 5'-gaataaaaagtctgtcttctgctcatagcgtcagcatcttctttgttgaatttttccttcatgt-3'
S382	a1144g, g1145c	5'-aagaagatgctgacgctatggccagaagacaggctttttatg-3' 5'-cataaaaagcctgtcttctggccatagcgtcagcatcttctt-3'
T386, S389	a1156g, t1165g	5'-agaagatactgacagtatggccagaagacaggctttttatgctaacaatcgaagcccaac-3' 5'-gttgggcttcgattgttagcataaaaagcctgtcttctggccatactgtcagtatcttct-3'
S393, T395	a1177g, g1178c, a1183g	5'-cacatacccgcagcgtttgctggggctcgattgttagcataaaaa-3' 5'-tttttatgctaacaatcgagccccagcaaacgctgcgggtatgtg-3'
S397, T398	a1189g, g1190c, a1192g	5'-aacaatcgaagcccaacaaacgctgcgggtatgtggaaggactc-3' 5'-gagtccttccacatacccgcagcgtttgttgggcttcgattgtt-3'
S404, S407, S408, S410	t1210g, t1219g, t1222g, t1228g	5'-cgggtatgtggaaggacgcgcctaaagctgccaaggccatcaaattcattcct-3' 5'-aggaatgaatttgatggccttggcagctttaggcgcgtccttccacatacccg-3'
S417, T418	t1249g, a1252g	5'-ccatcaaattcattcctgttgcagcttgactcgagtctagaggg-3' 5'-ccctctagactcgagtcaagctgcaacaggaatgaatttgatgg-3'

Supplemental Fig. 1: A) Heart rate to body weight ratios of TAC mice ± SR 49059. ***p<0.01, one-way ANOVA with Bonferroni multiple comparisons test (6 total comparisons). B) Serial changes in LV mass in response to TAC ± SR 49059 as determined by echocardiography. **p<0.01, ***p<0.001 TAC+V versus Sham+V, †p<0.05, ††p<0.01, †††p<0.001 TAC+SR versus Sham+V at corresponding weeks, two-way repeated measures ANOVA with Bonferroni multiple comparisons test (6 comparisons total). N = 9 (Sham+V), 8 (Sham+SR), 13 (TAC+V), 14 (TAC+SR). C) Summary of the changes in Ca^{2+} transients in adult mouse cardiomyocytes in response to increasing concentrations of AVP. N = 5 (0-100 nM AVP, 3 (1000 nM AVP).

Supplemental Fig. 2: A) AFVM infected with Ad-ICUE3 were stimulated with ISO (100nM) alone or following pretreatment with ICI 118,551 (β2AR-selective inhibitor, 100nM) or CGP 20712A (β1AR-selective inhibitor, 100nM). B) %AUC summary of the data in (A) indicating that the ISO-mediated cAMP increase observed in AFVM is predominantly β1AR-dependent. ***p<0.001, ns = not significant, one-way ANOVA with Bonferonni multiple comparisons test (3 comparisons total). N= 14 (ISO), 19 (ICI 118,551+ISO), 16 (CGP 20712A+ISO). Human U2S osteosarcoma cells infected with Ad-ICUE3 were stimulated with 1μM ISO in the absence or presence of increasing concentrations of ICI 188,551 (C) or CGP 20712A (D). Pretreatment with ICI completely abolished the ISO-mediated increase in cAMP generation, while CGP was only able to block the ISO effect at 10μM, indicating that ISO-mediated cAMP generation in U2S cells is predominantly β2AR-dependent. ***p<0.001, ns = not significant, one-way ANOVA with Bonferroni multiple comparisons test (21 comparisons total). N = 7 per treatment condition. E) U2S cells transfected with the diacylglycerol FRET reporter (DAGR) and HA-tagged V1AR were stimulated with 1μM AVP, showing a rapid DAG generation response to AVP in these cells. N = 26. F) U2S cells transfected with ICUE3 and V1AR were stimulated with increasing ISO concentrations ± 1μM AVP, revealing a concentration-dependent increase in ISO-mediated cAMP production that was not sensitive to AVP pretreatment. F) Concentration-response (%AUC) analysis demonstrate a lack of impact of V1AR signaling on β2AR-mediated cAMP generation in U2S cells (EC_{50} of ~16nM ISO in both the presence or absence of AVP). N = 7-10 per treatment condition.

Supplemental Figure 3: A) HEK 293 cells transfected with V1AR and DAGR were stimulated with increasing concentrations of AVP, with the concentration-response curve shown in (B). N = 8-24 per treatment condition. C) HEK 293 stably overexpressing AT1R and transfected with DAGR were stimulated with increasing concentrations of Ang II, with the concentration-response curve shown in (D). N = 20-60 per treatment condition. E) Pretreatment of HEK 293 cells expressing AT1R, β1AR and ICUE3 with Ang II (1μM) did not alter ISO (1nM)-mediated cAMP production, as summarized in (F). ns = not significant, two-tailed unpaired t-test. N = 21 (ISO), 22 (Ang II+ISO).

Supplemental Fig. 4: Radioligand binding of transiently transfected WT V1AR versus GRK$^-$V1AR in HEK 293 cells shows similar levels of expression (B_{max}, A) and ligand affinity (K_d, B). N = 3 each. Radioligand binding of WT versus V1AR-TG mouse heart membrane preparations shows a five-fold increase in V1AR expression in the V1AR-TG hearts over WT levels (C) with similar ligand affinities in each heart genotype (D). ***p<0.001, ns = not significant, two-tailed unpaired t-test. N = 5 each. Cardiac contractile parameters were measured in ex vivo Langendorff preparations from WT mice. Infusion of increasing concentrations of AVP led to a small decrease in contractility in WT hearts as measured by LVDP (E), +dP/dt (F) and –dP/dt (G), expressed as % of baseline. N = 3 hearts.

Supplemental Figure 1

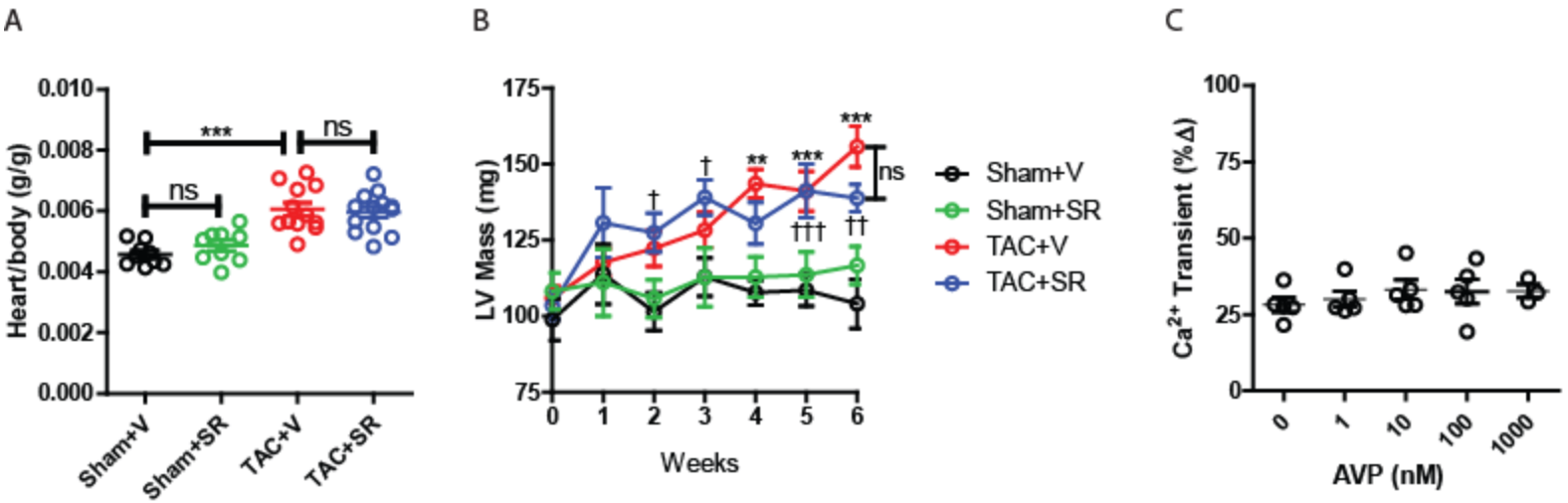

Supplemental Figure 2

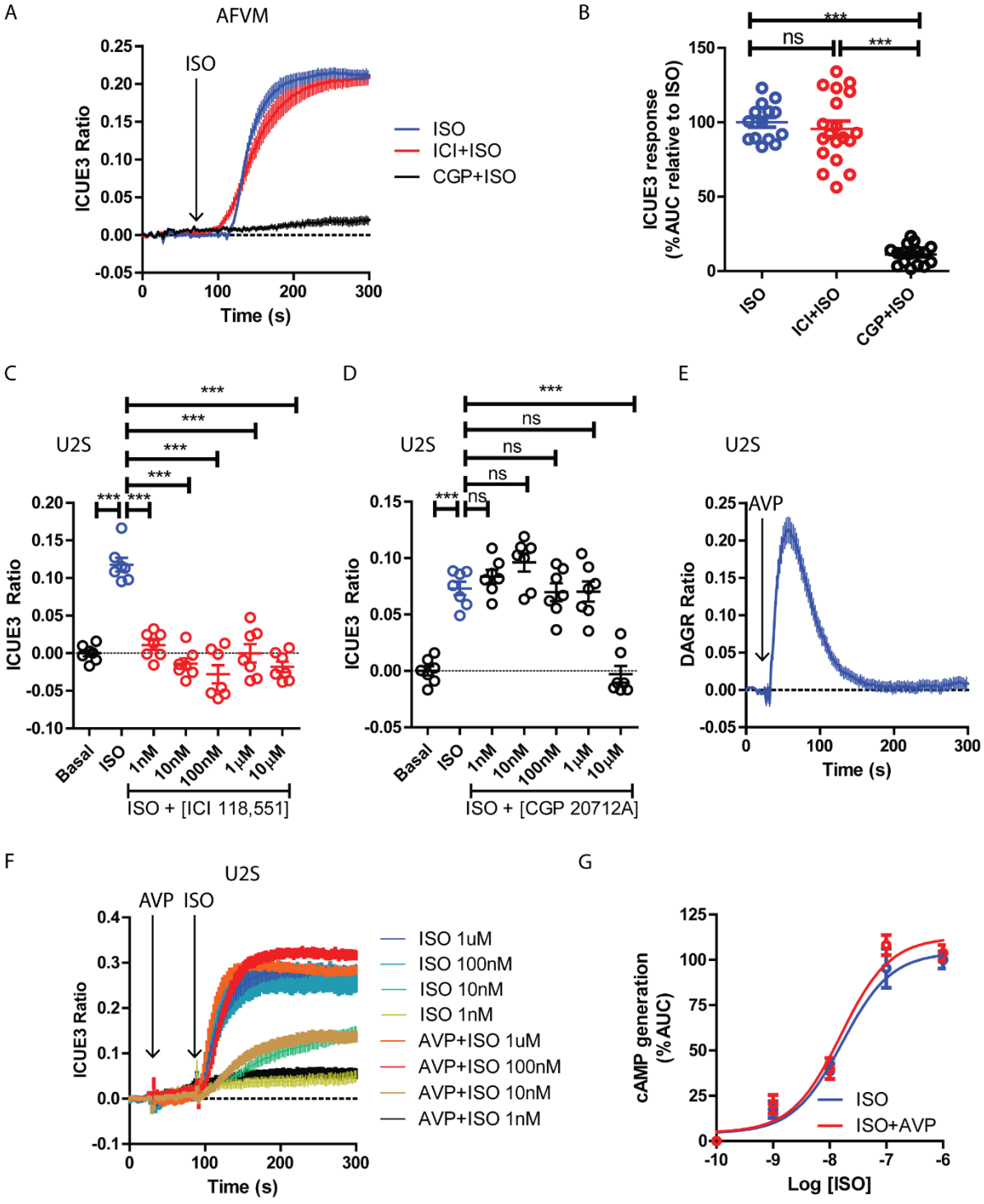

Supplemental Figure 3

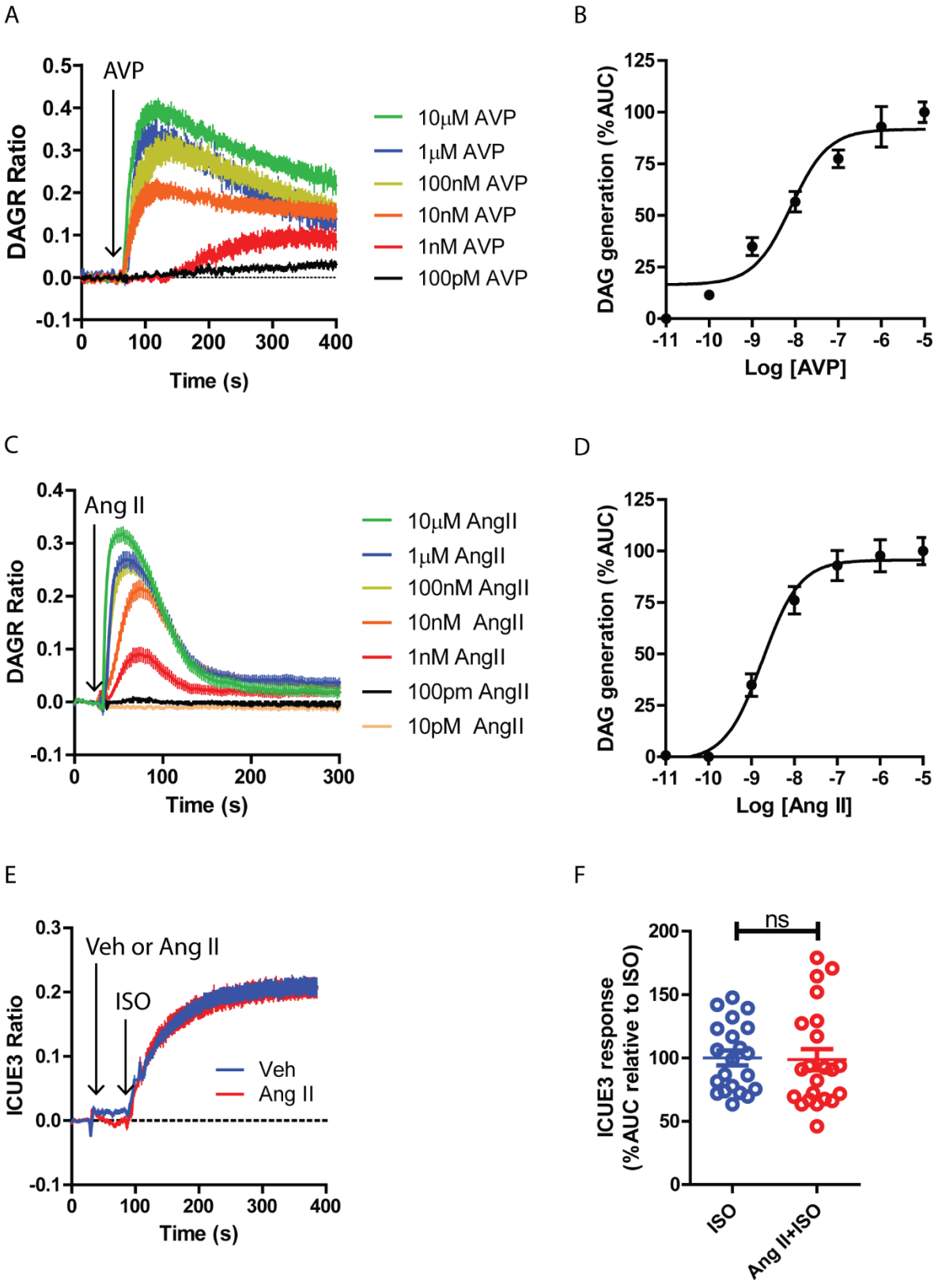

Supplemental Figure 4